

---

1 This manuscript is a EarthArxiv preprint and has been submitted for publication in GEOLOGY.  
2 Please note that the manuscript has not been peer-reviewed yet and that late versions of the  
3 manuscript may change slightly due to the review process. If accepted, the final version of the  
4 manuscript will be available via the 'Peer-reviewed Publication DOI' link on the right-hand side  
5 of this page. We welcome feedback, so please feel free to contact any of the authors.

---

6 Rift kinematics preserved in deep-time erosional landscape  
7 below the northern North Sea

8 **Thilo Wrona<sup>1,2\*</sup>, Alex Whittaker<sup>3</sup>, Rebecca E. Bell<sup>3</sup>, Robert L. Gawthorpe<sup>1</sup>, Haakon**  
9 **Fossen<sup>4</sup>, Christopher A-L. Jackson<sup>5</sup> and Marit Stokke Bauck<sup>6,7</sup>**

10 *<sup>1</sup>Department of Earth Science, University of Bergen, Allégaten 41, N-5007 Bergen, Norway*

11 *<sup>2</sup>GFZ German Research Centre for Geosciences, Telegrafenberg, 14473 Potsdam, Germany*

12 *<sup>3</sup>Department of Earth Science and Engineering, Imperial College, Prince Consort Road, London,*  
13 *SW7 2BP, UK*

14 *<sup>4</sup>Museum of Natural History, University of Bergen, Allégaten 41, N-5007, Bergen, Norway*

15 *<sup>5</sup>Department of Earth and Environmental Sciences, The University of Manchester, Williamson*  
16 *Building, Oxford Road, Manchester, M13 9PL, UK*

17 *<sup>6</sup>CGG, Lilleakerveien 6A, P.O.Box 43 Lilleaker, 0216 Oslo*

18 *<sup>7</sup>Department of Geosciences, University of Oslo, P.O. Box 1047 Blindern, N-0316 Oslo, Norway*

19 **ABSTRACT**

20 Our understanding of continental rifting is largely derived from the stratigraphic record.  
21 This archive is, however, incomplete as it does not capture the geomorphic and erosional record  
22 of rifting. New 3D seismic reflection data reveals a Late Permian-Early Triassic landscape  
23 incised into the pre-rift basement of the northern North Sea. This landscape, which covers at  
24 least 542 km<sup>2</sup>, preserves a drainage system bound by two major tectonic faults. A quantitative  
25 geomorphic analysis of the drainage system reveals 68 catchments, with channel steepness and  
26 knickpoint analysis of catchment-hosted paleo-rivers showing that the landscape preserved a >2

27 Myrs long period of transient tectonics. We interpret that this landscape records punctuated uplift  
28 of the footwall of a major rift-related normal fault at the onset of rifting. The landscape was  
29 preserved by a combination of relatively rapid subsidence in the hangingwall of a younger fault  
30 and burial by post-incision sediments. We show how and why erosional landscapes are preserved  
31 in the stratigraphic record, and how they can help us understand the tectono-stratigraphic  
32 evolution of ancient continental rifts.

### 33 **INTRODUCTION**

34 Tectonics, landscape evolution, and stratigraphy are closely coupled in active continental  
35 rifts (e.g. Cowie et al., 2000; Gawthorpe and Leeder, 2000). Growing normal faults influence the  
36 geometry of drainage networks and incision rates within upland catchments, which in turn  
37 controls the location, magnitude, and routing of sediment supply to neighbouring depocenters  
38 (Cowie et al., 2006; Whittaker et al., 2010). This coupling means that the transient erosional  
39 response of fluvial landscapes to rifting can be used to record the timescales, throw rates and  
40 kinematics of active faulting over a range of spatial scales (e.g. Kirby and Whipple, 2012;  
41 Whittaker and Boulton, 2012). In modern rifts, we can analyse digital elevation models (DEMs),  
42 together with independent tectonic and stratigraphic constraints, to estimate the patterns and rates  
43 of fault evolution (e.g. Pechlivanidou et al., 2018; Watkins et al., 2020; Quye-Sawyer et al.,  
44 2021), but in many ancient rifts similar rift-related paleo-landscapes are absent. Consequently,  
45 time-averaged patterns of faulting must be reconstructed indirectly from structural measurements  
46 and stratigraphic observations (e.g. Gawthorpe and Leeder, 2000, Kent et al., 2017). If paleo-  
47 landscapes can be found in the stratigraphic record of ancient rifts, they may reveal important  
48 new information about fault behaviour.

49 To our knowledge, the oldest palaeo-landscapes ever found are 55-58 Ma, seismically imaged  
50 drainage networks found of the coast of Scotland, UK, developed and preserved in response to  
51 Iceland plume-driven uplift and subsidence (Hartley et al., 2011; Stucky de Quay et al., 2017).  
52 Here, we present a new candidate for the oldest ever complete landscape yet described from the  
53 geological record, defined by an erosional surface carved into the Paleozoic basement of the  
54 northern North Sea rift, offshore Norway, imaged in 3D seismic reflection data (Text S1, S2 in  
55 the Data Repository). The surface covers at least c. 542 km<sup>2</sup> and reveals a drainage system that  
56 developed at the onset of Permian-Triassic rifting (~261±10 Ma; Fossen & Dunlap, 1999). A  
57 quantitative geomorphic analysis of the surface shows that this drainage system contains an  
58 exceptional record of the transient landscape response to incipient faulting, from which we  
59 deduce the history and timescales of rift-related normal faulting. Our work shows how paleo-  
60 surfaces imaged in 3D seismic reflection data can provide crucial insights into the tectono-  
61 stratigraphic evolution of ancient continental rifts.

## 62 **GEOLOGICAL SETTING**

63 The study area is located in the northern North Sea rift (Fig. 1A). An up to 12 km thick  
64 syn- and post-rift sedimentary succession was deposited on crystalline basement during and after  
65 Late Permian-Early Triassic and Middle Jurassic-Early Cretaceous rifting (Færseth, 1996; Bell et  
66 al., 2014; Maystrenko et al., 2017). In the Late Permian-Early Triassic, E-W extension led to the  
67 development of large (>100 km long) normal faults, such as the W-dipping Vette and Øygarden  
68 faults, which bound half-grabens and are the focus of this study (Fig. 1B). By the Triassic, these  
69 faults had developed large displacements (up to 4 km) and were associated with relatively high  
70 slip rates (0.1–0.15 mm/yr); however, the relative age of these faults remains unknown. The top

71 of the basement in the footwall of the Vette Fault is capped by a distinct erosional surface (Fig.  
72 1B), which we describe and analyse below. Upper Permian and Lower Triassic sequences  
73 capping this surface comprise alluvial and fluvial rocks (Evans, 2003).

## 74 **METHODS**

### 75 **3D seismic interpretation**

76 We use broadband 3D seismic reflection data to map the top of the acoustic basement at a  
77 spatial resolution of 12.5×18.5 m, revealing a landscape preserved in the footwall of the Vette  
78 Fault (Figs. 1, S1). The top of the acoustic basement is a high-amplitude reflection originating  
79 from the impedance contrast between sedimentary rocks (above) and crystalline basement  
80 (below). To analyse the geomorphology of this surface, we create a DEM by restoring it to its  
81 original geometry, removing the effects of subsequent burial, fault block rotation, and post-rift  
82 tilting (Text S3; Figs. S1, S2) (cf. Hartley et al., 2011; Stucky de Quay et al., 2017). We also  
83 map two seismically distinct, wedge-shaped Permian-Triassic units to understand the  
84 preservation of the landscape (Unit 1 showing medium-to-low amplitude, sub-horizontal layering  
85 and Unit 2; characterised by chaotic, discontinuous low amplitudes (e.g. Fig. 1B).

### 86 **Geomorphic analysis**

87 We perform a quantitative analysis of the restored DEM using TopoToolbox 2  
88 (Schwanghart and Scherler, 2014) and recover stream networks and river long profiles using a  
89 D8 flow routing algorithm with a flow accumulation threshold of 0.25 km<sup>2</sup> (e.g. Whittaker and  
90 Boulton, 2012). As the derivation of a stream network requires a consistent hydrological surface,  
91 pits in the reconstructed DEM must be filled. Since this aims to remove erroneous elevation

92 values, we use the seismic resolution (18 m) as the maximum filling depth. We provide full  
93 details on our workflow in the supplementary material (Figs. S3, S4). Because rivers and streams  
94 perturbed by tectonic uplift often show steep segments in their elevation profiles (e.g. Kirby and  
95 Whipple, 2012), we calculate the normalized channel steepness of the fluvial network (e.g.  
96 Schwanghart and Scherler, 2014) (Fig. 2B, Text S4).

97 To investigate any preserved transient landscape responses to normal faulting, we  
98 identify knickpoints in the palaeo-river long profiles of our stream network using the  
99 TopoToolbox 2 with a knickpoint finder tolerance 2.5 times the seismic resolution of our survey  
100 (45 m) (Text S5, Figs. S5, S6). This high tolerance assures that we extract only major  
101 knickpoints in the network (Fig. 2C, D, Figs. S5, S6). We measured the elevation of these  
102 knickpoints relative to the Vette Fault to a precision of  $\pm 25$  m, and their distance upstream with  
103 a precision of  $\pm 100$  m (Tab. S1). Knickpoint height relative to the fault was compared to  
104 geologic constraints on fault throw (c.f. Bell et al., 2014) and knickpoint locations were  
105 compared to palaeo-catchment drainage area. For knickpoints located upstream of the footwall-  
106 bounding Vette Fault, we estimate a potential timescale for their propagation upstream, assuming  
107 they started from the fault, using the propagation velocity,  $V$ , derived from a unit stream power  
108 erosion law (Tucker and Whipple, 2002) (Text S6) and data compilations upstream of modern  
109 active faults (Whittaker and Boulton, 2012; Kent et al., 2018).

## 110 **RESULTS**

### 111 **Seismic and geomorphic expression of the palaeo-landscape**

112 Our study area covers an area of  $\sim 542 \text{ km}^2$  and is located between the Vette and the  
113 Øygarden faults (Fig. 1). The surface is carved into basement rocks regionally consisting of  
114 Devonian sediments, Caledonian allochthons, and Proterozoic crust (Fazlikhani et al., 2017). In  
115 cross-section, the surface is highly irregular, showing relatively steep slopes (up to  $15^\circ$ ) and  
116 moderate relief ( $< 800 \text{ m}$ ) (Fig. 1B). This seismically defined morphology, combined with our  
117 subsequent geomorphic analysis (Fig. 2) and the depositional setting of the overlying, non-  
118 marine Triassic rocks filling and preserving the unconformity surface, are very strong evidence  
119 that the surface represents a subaerial landscape.

120 Our DEM analysis of the surface reveals an intricate 3D landscape showing a small fault-  
121 bounded mountain range with relief up to  $800 \text{ m}$ , cut by a dendritic fluvial network, from which  
122 individual catchments can be identified with exceptional clarity (Fig. 2A). Consequently, our  
123 results depict a possibly unique snapshot of an ancient footwall landscape, which based on the  
124 available age must have formed during slip accumulation on the Vette Fault.

### 125 **Landscape response to active faulting at 250 Ma**

126 We extracted 68 palaeo-catchments with drainage areas up to  $60 \text{ km}^2$  from the DEM  
127 (Tab. S1). The longest trunk rivers are up to  $20 \text{ km}$  long. Many catchments show abrupt channel  
128 steepness index variations (Fig. 2B). For instance, high steepness index river segments ( $> 50 \text{ m}$   
129 long) are mainly found in catchments that decrease in elevation and appear to drain westwards  
130 towards the Vette Fault, (Fig. 2B) (Tabs. S1, 2). Reconstructed palaeo-channel long profiles are

131 *not* concave up, but show distinct convexities on a range of length scales (Fig. 3A). The channel  
132 geometries are remarkably similar to those observed in modern fluvial systems draining across  
133 active normal faults (c.f. Whittaker, 2012). Consequently the sharp variations in channel  
134 steepness suggest that the palaeo-landscape was not in a topographic steady state when  
135 preserved.

136 Numerous knickpoints are visible on many of the paleo-river long profiles; we extract  
137 those that pass our filtering threshold (Figs. 2C, 3A). Thirteen catchments have at least one  
138 significant knickpoint upstream of the Vette Fault and several have two (Tabs. S1, S2) (Fig. 3A).  
139 These knickpoints lie at distances between 0.44-10 km upstream of the Vette Fault, with  
140 elevations for the lower or single set of knickpoints varying between 45->300 m (Fig. 3B, C),  
141 considerably lower than the overall relief of the palaeo-landscape (Fig. 2). In terms of their size  
142 and scale, these catchments and knickpoints are comparable to modern fluvial systems crossing  
143 faults in Italy, Turkey, and Greece (Whittaker and Boulton, 2012; Whittaker and Walker, 2015;  
144 Roda-Boluda and Whittaker, 2017), where rivers have been shown to record changing fault slip  
145 rates over timescales of 1-5 million years.

146 When plotted along the strike of the Vette Fault, (Fig 3) knickpoint elevation for both sets  
147 of knickpoints relative to the fault is an order of magnitude smaller than the fault throw between  
148 0-40 km along strike, with these values being comparable for the northern part of the fault.  
149 Knickpoint elevations are smallest 25-40 km along strike, which is where throw is presently  
150 greatest (Fig. 3). Given that knickpoint elevation, since formation, scales predictably with fault  
151 slip rate (c.f. Whittaker and Walker, 2015), we infer that along-strike changes in elevation define  
152 two paleo fault segments that were active early in the evolution of the Vette Fault. The upper set



153 of knickpoints also have elevations that are considerably less than the geologic throw. Although  
154 there is some scatter, single knickpoints on paleo-catchments with bigger drainage areas are  
155 located predictably further upstream, ( $L \sim A^{0.38 \pm 0.12}$ ) (Fig. S7) which is consistent with them  
156 forming at a similar time. Consequently, we interpret these knickpoints to capture the transient  
157 response of the footwall landscape to the early growth of the Vette Fault near the onset of rifting.  
158 The palaeo-landscape was subsequently buried in the hanging wall of the Øygarden Fault before  
159 the transient tectonic signal had a chance to propagate fully through the fluvial system.

## 160 **DISCUSSION & CONCLUSIONS**

### 161 **Preserved landscape – transient tectonics**

162 Our study reveals a subaerial drainage system carved into the footwall of the Vette Fault,  
163 northern North Sea Rift (Fig. 1). The overlying stratigraphy indicates that this landscape  
164 developed during Permian-Triassic rifting. Our geomorphic analysis of the system reveals that  
165 many catchments draining across the Vette Fault have high steepness indices (Fig. 2B), and that  
166 13 of the 68 catchments have knickpoints, which are indicative of an increase in tectonic uplift  
167 rates (Fig. 2C) (*sensu* Hartley et al., 2011; Stucky de Quay et al., 2017). The seismically imaged  
168 paleo-rivers thus capture the landscape response to footwall uplift, generated by growth of the  
169 Vette Fault around 250 Ma. The presence of two sets of knickpoints reflects changing fault slip  
170 rates during the early evolution of the fault. This likely reflects throw rate increases driven by  
171 fault growth and perhaps linkage, evidenced by the fact that the lower set of knickpoints records  
172 two, presumably unlinked, paleo segments. This is the first time that the geomorphic response of  
173 catchments to active fault growth and interaction has been reconstructed and mapped in an  
174 ancient rift.

## 175 **Duration of faulting and knickpoint migration**

176           Once formed, knickpoints migrate upstream, as catchments progressively respond to the  
177 relative change in base level (Kirby and Whipple, 2012). We can thus use the duration of  
178 knickpoint migration upstream of the Vette Fault as a proxy for the time of fault activity.  
179 Knickpoint elevation upstream of interacting fault segments is known to scale with the relative  
180 difference in throw rates and the time since this has taken place (Whittaker & Boulton, 2012).  
181 The maximum elevation of the lower knickpoints is ~250 m. If we divide this by published  
182 time-averaged throw rates on the Vette Fault of 0.15 mm/yr (Bell et al., 2014) as a maximum,  
183 this would imply that the transient landscape represents a minimum of 1.7 Myrs, similar to  
184 faulted landscapes in Greece (e.g. Whittaker and Walker, 2015). Alternatively, if we calculate  
185 upstream migration of the knickpoints using bedrock erodibilities based on an average of a  
186 compilation of modern systems upstream of active faults with similar drainage areas and slip  
187 rates (see Methods) we obtain a preferred median landscape response time of 2.1 Myrs and  
188 extremes of a 1.1 to 10.1 Myrs; this suggests that the paleo-landscape records fault growth and  
189 interaction over periods >2 Myrs (Fig. 4C). Considering that dating of sedimentary rocks, fault  
190 rocks, and dykes suggest that Permian-Triassic rifting began between 261±10 (Fossen & Dunlap,  
191 1999) and lasted tens of millions of years (Ravnås et al., 2000), our results indicate that the Vette  
192 Fault was only active for a fraction of this episode.

## 193 **Landscape preservation – strain migration**

194           Erosional landscapes, such as the one described here, are not usually preserved in the  
195 stratigraphic record, despite undoubtedly forming throughout the history of Earth. To understand  
196 its preservation, we reconstruct the tectono-stratigraphic context and evolution of the system  
197 through time (Fig. 4). The landscape developed at the onset of rifting in the northern North Sea,

198 when the young Vette Fault initiated, and when Permian-Triassic strata (Unit 1) were being  
199 deposited in its immediate hanging wall (Fig. 4A). The knickpoints and overall landscape were  
200 created when segments of the Vette Fault were displacing paleo-streams and rivers (Fig. 2C).  
201 Subsequently, the drainage system was rapidly buried and preserved beneath Permian-Triassic  
202 strata (Unit 2) (Figs. 1B, 4B). This period lasted c. 2 Myrs. The rapid burial of the footwall of  
203 the Vette Fault, before the transient landscape had equilibrated, was likely driven by strain  
204 migration from the Vette Fault to the Øygarden Fault, with the hanging wall of the former  
205 producing subsidence that outpaced footwall uplift on the Vette Fault.

## 206 **ACKNOWLEDGMENTS**

207 We thank VISTA, UiB, ESM and Geo.X for financial support and CGG for access to this  
208 3D seismic dataset.

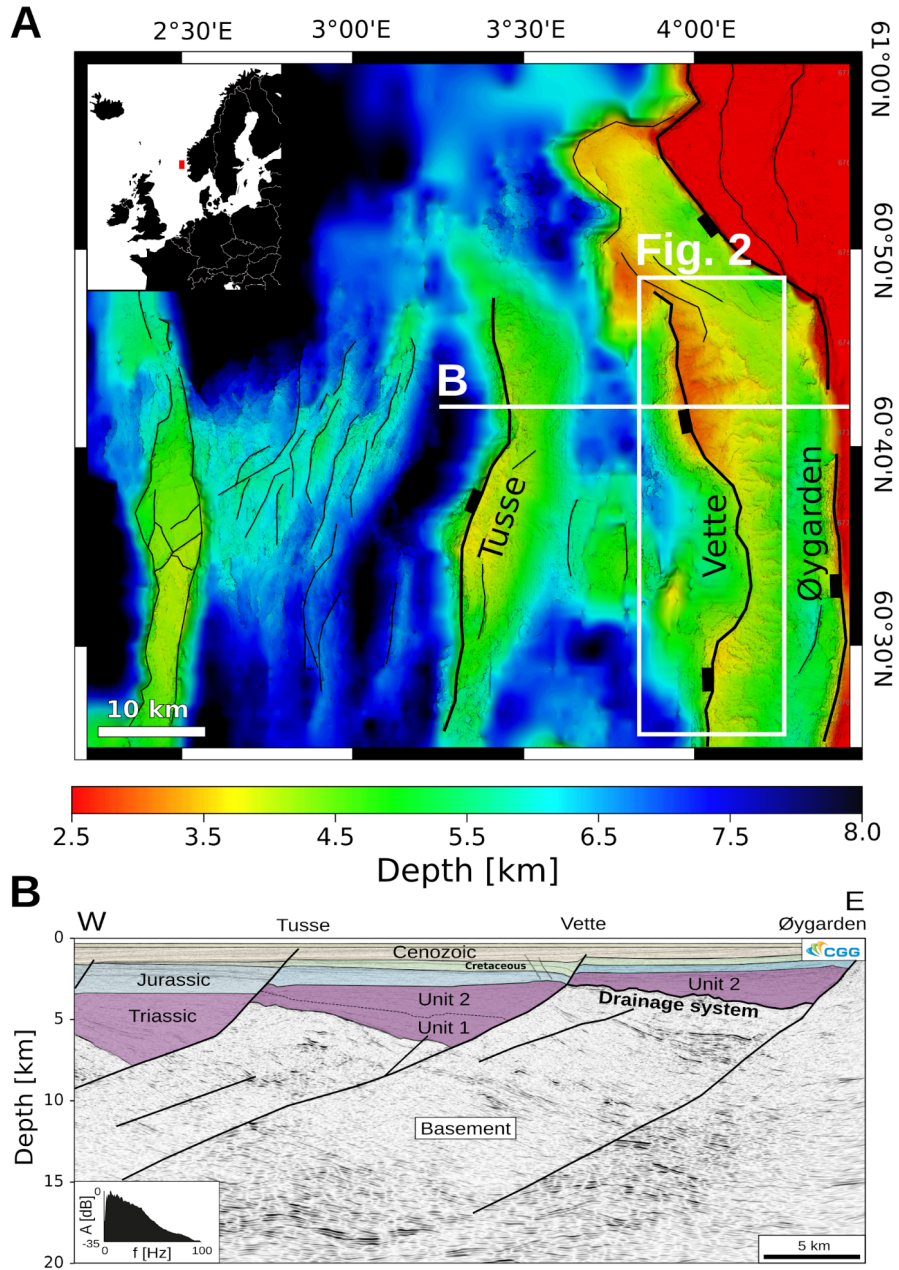
## 209 **REFERENCES CITED**

- 210 Bell, R. E., Jackson, C. A. L., Whipp, P. S., & Clements, B. (2014). Strain migration during  
211 multiphase extension: Observations from the northern North Sea. *Tectonics*, 33(10), 1936–1963.  
212 <https://doi.org/10.1002/2014TC003551>
- 213 Cowie, P. A., Attal, M., Tucker, G. E., Whittaker, A. C., Naylor, M., Ganas, A., & Roberts, G. P.  
214 (2006). Investigating the surface process response to fault interaction and linkage using a  
215 numerical modelling approach. *Basin Research*, 18(3), 231–266. <https://doi.org/10.1111/j.1365-2117.2006.00298.x>
- 217 Cowie, P. A., Gupta, S., & Dawers, N. H. (2000). Implications of fault array evolution for synrift  
218 depocentre development: insights from a numerical fault growth model. *Basin Research*, 12(3–  
219 4), 241–261. <https://doi.org/10.1046/j.1365-2117.2000.00126.x>
- 220 Cowie, Patience A., Whittaker, A. C., Attal, M., Roberts, G., Tucker, G. E., & Ganas, A. (2008).  
221 New constraints on sediment-flux-dependent river incision: Implications for extracting tectonic  
222 signals from river profiles. *Geology*. <https://doi.org/10.1130/G24681A.1>

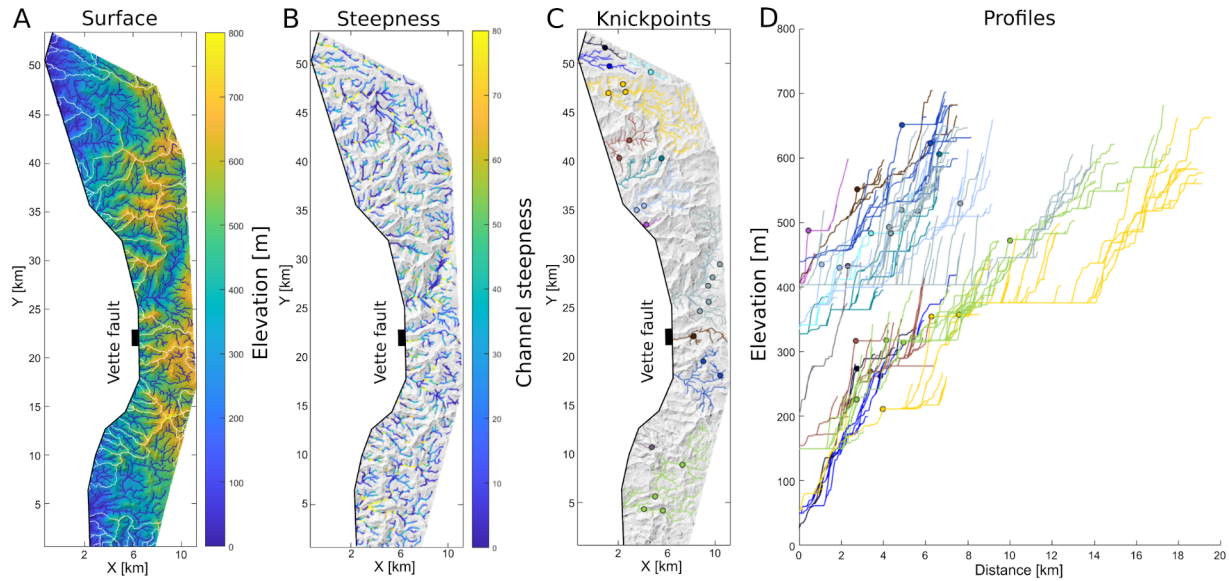
- 223 Evans, D. (2003). The Millennium Atlas: Petroleum Geology of the Central and Northern North  
224 Sea; [A Project of the Geological Society of London, the Geological Survey of Denmark and  
225 Greenland and the Norwegian Petroleum Society].
- 226 Færseth, R. B. (1996). Interaction of permo-triassic and jurassic extensional fault-blocks during  
227 the development of the northern North Sea. *Journal of the Geological Society*, 153(6), 931–944.  
228 <https://doi.org/10.1144/gsjgs.153.6.0931>
- 229 Fazlikhani, H., Fossen, H., Gawthorpe, R. L., Faleide, J. I., & Bell, R. E. (2017). Basement  
230 structure and its influence on the structural configuration of the northern North Sea rift.  
231 *Tectonics*, 36(6), 1151–1177. <https://doi.org/10.1002/2017TC004514>
- 232 Gawthorpe, R. L., & Leeder, M. R. (2000). Tectono-sedimentary evolution of active extensional  
233 basins. *Basin Research*, 12(3–4), 195–218. [https://doi.org/DOI 10.1046/j.1365-  
234 2117.2000.00121.x](https://doi.org/DOI%2010.1046/j.1365-2117.2000.00121.x)
- 235 Hartley, R. A., Roberts, G. G., White, N., & Richardson, C. (2011). Transient convective uplift  
236 of an ancient buried landscape. *Nature Geoscience*, 4(8), 562–565.  
237 <https://doi.org/10.1038/ngeo1191>
- 238 Kent, E., Boulton, S. J., Whittaker, A. C., Stewart, I. S., & Cihat Alçiçek, M. (2017). Normal  
239 fault growth and linkage in the Gediz (Alaşehir) Graben, Western Turkey, revealed by transient  
240 river long-profiles and slope-break knickpoints. *Earth Surface Processes and Landforms*, 42(5),  
241 836–852. <https://doi.org/10.1002/esp.4049>
- 242 Kirby, E., & Whipple, K. X. (2012). Expression of active tectonics in erosional landscapes.  
243 *Journal of Structural Geology*, 44, 54–75. <https://doi.org/10.1016/j.jsg.2012.07.009>
- 244 Lenhart, A., Jackson, C. A. L., Bell, R. E., Duffy, O. B., Gawthorpe, R. L., & Fossen, H. (2019).  
245 Structural architecture and composition of crystalline basement offshore west Norway.  
246 *Lithosphere*, 11(2), 273–293. <https://doi.org/10.1130/L668.1>
- 247 Maystrenko, Y. P., Olesen, O., Ebbing, J., & Nasuti, A. (2017). Deep structure of the northern  
248 north sea and southwestern Norway based on 3D density and magnetic modelling. *Norsk  
249 Geologisk Tidsskrift*, 97(3), 169–210. <https://doi.org/10.17850/njg97-3-01>
- 250 Pechlivanidou, S., Cowie, P. A., Hannisdal, B., Whittaker, A. C., Gawthorpe, R. L., Pennos, C.,  
251 & Riiser, O. S. (2017). *Source-to-sink analysis in an active extensional setting: Holocene  
252 erosion and deposition in the Sperchios rift, central Greece*. <https://doi.org/10.1111/bre.12263>

- 253 Quye-Sawyer, J., Whittaker, A. C., Roberts, G. G., & Rood, D. H. (2021). Fault Throw and  
254 Regional Uplift Histories From Drainage Analysis: Evolution of Southern Italy. *Tectonics*, 40(4).  
255 <https://doi.org/10.1029/2020tc006076>
- 256 Roda-Boluda, D. C., & Whittaker, A. C. (2017). Structural and geomorphological constraints on  
257 active normal faulting and landscape evolution in Calabria, Italy. *Journal of the Geological*  
258 *Society*, 174(4), 701–720. <https://doi.org/10.1144/jgs2016-097>
- 259 Schwanghart, W., & Scherler, D. (2014). Short Communication: TopoToolbox 2 - MATLAB-  
260 based software for topographic analysis and modeling in Earth surface sciences. *Earth Surface*  
261 *Dynamics*, 2(1), 1–7. <https://doi.org/10.5194/esurf-2-1-2014>
- 262 Stucky de Quay, G., Roberts, G. G., Watson, J. S., & Jackson, C. A. L. (2017). Incipient mantle  
263 plume evolution: Constraints from ancient landscapes buried beneath the North Sea.  
264 *Geochemistry, Geophysics, Geosystems*, 18(3), 973–993. <https://doi.org/10.1002/2016GC006769>
- 265 Ter Voorde, M., Færseth, R. B., Gabrielsen, R. H., & Cloetingh, S. A. P. L. (2000). Repeated  
266 lithosphere extension in the northern Viking Graben: A coupled or a decoupled rheology?  
267 *Geological Society Special Publication*, 167(1), 59–81.  
268 <https://doi.org/10.1144/GSL.SP.2000.167.01.04>
- 269 Tucker, G. E., & Whipple, K. X. (2002). Topographic outcomes predicted by stream erosion  
270 models: Sensitivity analysis and intermodel comparison. *Journal of Geophysical Research: Solid*  
271 *Earth*, 107(B9), ETG 1-1-ETG 1-16. <https://doi.org/10.1029/2001jb000162>
- 272 Watkins, S. E., Whittaker, A. C., Bell, R. E., S Brooke, S. A., Ganti, V., Gawthorpe, R. L.,  
273 McNeill, L. C., Nixon, C. W., & Stephen Watkins, C. E. (2020). Straight from the source's  
274 mouth: Controls on field-constrained sediment export across the entire active Corinth Rift,  
275 central Greece. *1600 | Basin Research*, 32, 1600–1625. <https://doi.org/10.1111/bre.12444>
- 276 Whittaker, A. C., Attal, M., & Allen, P. A. (2010). Characterising the origin, nature and fate of  
277 sediment exported from catchments perturbed by active tectonics. *Basin Research*, 22(6), 809–  
278 828. <https://doi.org/10.1111/j.1365-2117.2009.00447.x>
- 279 Whittaker, A. C., & Boulton, S. J. (2012). Tectonic and climatic controls on knickpoint retreat  
280 rates and landscape response times. *Journal of Geophysical Research: Earth Surface*, 117(2).  
281 <https://doi.org/10.1029/2011JF002157>
- 282 Whittaker, A. C., & Walker, A. S. (2015). Geomorphic constraints on fault throw rates and  
283 linkage times: Examples from the Northern Gulf of Evia, Greece. *Journal of Geophysical*  
284 *Research F: Earth Surface*, 120(1), 137–158. <https://doi.org/10.1002/2014JF003318>

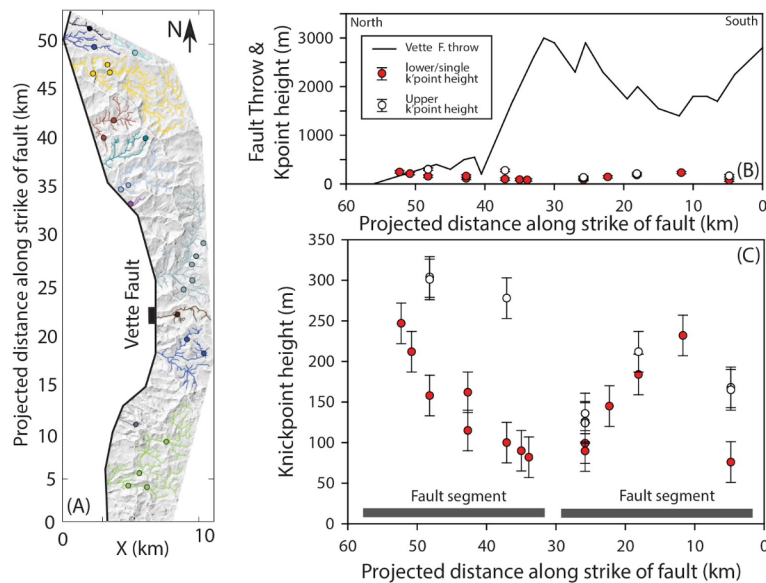
285 Ziegler, P. A. (1982). Triassic rifts and facies patterns in Western and Central Europe.  
286 *Geologische Rundschau*, 71(3), 747–772. <https://doi.org/10.1007/BF01821101>



288 Figure 1. A Basement surface showing rift-related normal faults and drainage system in the  
 289 northern North Sea. B Seismic section showing the drainage systems situated on top of the  
 290 basement. Permian-Triassic strata overlying the surface consists of two wedge-shaped units  
 291 Seismic data courtesy of CGG.

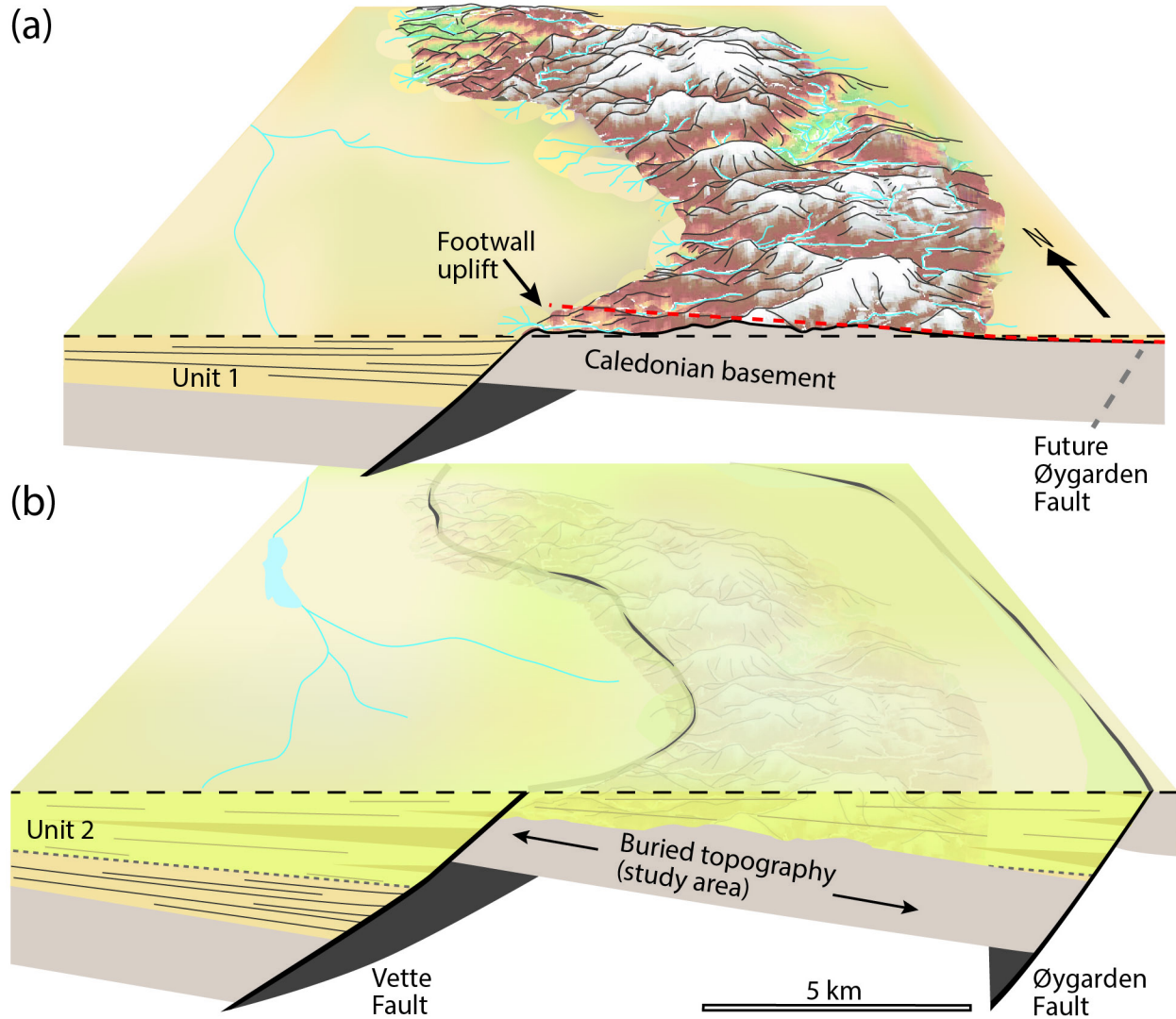


292 Figure 2. A Restored basement surface with stream network and drainage divides. B Normalized  
 293 channel steepness index of stream network. C Knickpoints extracted from stream network.



294 Figure 3: A Knickpoints extracted from stream network. B. Knickpoint height and fault throw  
 295 along strike (same scale). C Knickpoint height with error bar. Note the two populations of  
 296 knickpoints (upper-white and lower-red).





297 Figure 4: 3D diagram illustrating landscape evolution at the onset of rifting. A Landscape  
 298 development at the onset of rifting in the northern North Sea, when the young Vette Fault  
 299 initiated and Permian-Triassic strata (Unit 1) were being deposited in its immediate hanging  
 300 wall. Knickpoints creation when segments of the Vette Fault were displacing paleo-streams and  
 301 rivers as they grew, interacted and built footwall relief. B Subsequent subsidence and rapid burial  
 302 underneath Permian-Triassic strata (Unit 2) leading to landscape preservation.